Analysis and Operation of an Integrated Battery Charger Using the EV Traction Motor as Filter

Alisson Mengatto and Joselito A. Heerdt
Santa Catarina State University - UDESC
Electric Power Processing Group - nPEE
89.219-710, Joinville - SC, Brazil
alisson_mengatto@hotmail.com, joselito.heerdt@udesc.br

***Abstract*—This paper presents an operation mode for an onboard integrated battery charger (IBC) which uses the electric vehicle (EV) traction motor as input filter in the battery charging mode. The studied charger adds few components to the already existing power electronics employed for propulsion. By connecting the single-phase mains to the traction inverter, only two mechanical switches or solid state relays are necessary to configure the same converter to operate as a battery charger. The proposed operation mode for this IBC reduce and distribute the inverter losses during charging operation mode. Furthermore, a machine analysis is presented to characterize the machine behavior considering the single-phase input current flowing through the three-phase traction motor. Although the IBC is best suited for an induction motor (IM) application, an analysis of the feasibility of using a permanent magnet (PM) motor is realized. Simulation results are presented which validates the functionality of the proposed charger operation.**

***Keywords* – Electric Vehicle, Integrated Battery Charger, Stationary Reference Frame, Traction Motor, Vehicle-to-Grid.**

I. Introduction

Solutions for decreasing dependency on fossil fuel have gained attention in the last decade for many climate factors. Electric and plug-in hybrid electric vehicles (PHEV) are one of the alternatives for reducing CO_2 emissions, but they still need developments in infrastructure, chargers, and batteries to reduce costs and achieve mass adoption [1].

An integrated battery charger consists in the idea of reusing some of the built-in electrical components employed for traction in battery charging mode, as they are not used when the vehicle is at standstill. Significant reduction of mass, volume and costs are obtained, which consequently raises reliability and global efficiency of the vehicle. The onboard charger (OBC) power capacity is not anymore a constraint as the propulsion system has high-power specs compared with conventional EV chargers.

Different configurations of IBCs have been proposed in literature. Some authors integrated the entire drivetrain (i.e., used the motor inductances) [2] or only the power electronics components [3]. Beyond that, almost all commercially EVs today have regenerative braking capability to enhance efficiency, which needs bidirectional converters, so, integration of the dc-dc converter is also possible [4]. Other authors focused on the vehicle auxiliary battery, utilizing only one dc-dc converter with multiple outputs for charging both propulsion and auxiliary battery [5]. Moreover, as reviewed by [6], different solutions can also be classified by the quantity of extra components added, charging isolation or whether the grid is single or three-phase.

978-1-5090-6248-5/17/$31.00

Integration of propulsion and charger power electronics using the motor inductances were considered more than 30 years ago by Thimmesch with NASA [7], when mostly commutated converters were based on thyristors. However, their solution used the motor leakage inductance only as an in-rush limiter and low-frequency filter to the diode bridge rectifier formed by the anti-parallel thyristor switches of the inverter. A second stage composed by complex resonant circuits was used for charging. Furthermore, the single-phase ac source was placed in parallel with a mechanical relay used to disconnect one phase of the motor from one thyristor leg.

Other patents of single-phase integrated chargers were introduced for vehicles with one or more electrical machines [2], [8]. The first patented IBC [2] was based on a delta connected motor employing the leakage inductance for a boost rectifier using two legs of the VSC. No mechanical relays were used but an additional diode rectifier bridge was necessary.

A solution similar to [7], but using high-frequency switches was patented by [9] as showed by Fig 1a. During charging operation, a mechanical switch disconnects one of the three motor phases and the ac grid is placed in parallel with it. However, high-frequency switches were used to form a full-bridge rectifier with two legs of the propulsion inverter wherein the ac source and its EMI filter are placed in series with leakage inductances of two motor phases in order to establish a high-frequency input filter. Control signals to the other inverter leg left maintain the switches in off condition not providing current to the winding connected to this leg.

Another type of IBC which consists of connecting a single-phase diode bridge rectifier to the neutral point of the motor was introduced by Solero [10] and studied by [11] and [12]. In charging mode, the three-phase VSC and the motor leakage inductances are used to boost the rectified input voltage. Interleaving and instantaneous zero-torque, regardless of motor type and rotor position can be achieved by this configuration. However, access to the neutral point is not available in majority of motors and the motor configuration provides low equivalent

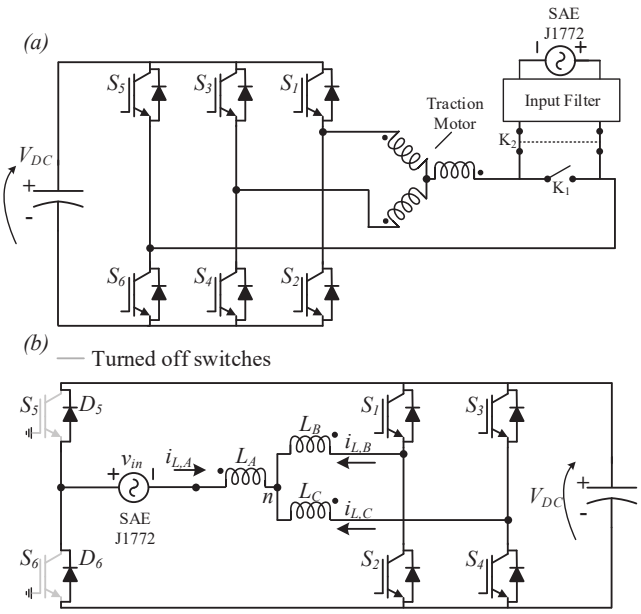

Fig. 1. Studied integrated battery topology [9]. (a) Conventional representation. (b) Alternative representation of the IBC topology. Reference adopted in motor operation for direction of current variables i_L are maintained.

inductance which may require an additional inductor, specially in high-power traction motors where the leakage inductance has low value.

The presented integrated charger topology of this paper is based on the patented by [9]. However, a different operation for this converter is proposed in order to make full use of the already existing power electronics devices. All legs of the inverter and all phases of the motor are employed as a single-phase rectifier converter able to reduce the conduction losses comparing with the original idea presented in the patent. Interleaving can be used to smooth the input current and double the input filter frequency. High equivalent inductance is expected comparing with solution of [10] and no special requirements are needed concerning the motor to be used.

Tipically, single-phase chargers do not develop torque in induction motors applied for IBC operation, but depending on rotor position in a PM synchronous motor (PMSM) instantaneous torque may be present. As this study is not provided by other references specific for the studied IBC, it is shown analytically by means of machine equations. The proposed operation mode is detailed in Section II as well as the minimum motor equivalent inductance required to keep the converter in continuous conduction mode (CCM) during charging. Section III presents an analysis for the mainly used motor types for EV traction. Finally, simulation results of the presented charger are provided in Section IV to validate the operation mode and torque equations applied in an induction motor real model.

II. Proposed Operation Mode for the Integrated Charger Topology

As an IBC based on a boost rectifier, it is only capable of providing a dc voltage higher than the peak value of single-phase ac voltage, i.e., is a step-up ac-dc converter. To adapt the battery voltage and reduce the current and voltage ripple usually a dc-dc converter is adopted as second-stage in the propulsion drive. The output dc voltage could be referred as the battery voltage in case of a single stage charger, or as dc link voltage if a second stage dc-dc converter exist. Here, this voltage will be called dc bus voltage to establish a pattern as the studied converter can be applied in both cases.

The EV propulsion converter is modified to provide a battery charging mode by placing a mechanical switch in one of the motor phases and connecting a sinusoidal voltage source in parallel with the relay K_1 as shown in Fig 1a, and redrawed in Fig 1b. Instead of operating with only two legs of the converter to form a full-bridge topology, providing zero voltage gating sinals to one of the S_1, S_2 or S_3, S_4 legs, as [9], all VSC legs have a path for current. The switches with the phase winding disconnected (S_5, S_6) are blocked and based on the input voltage polarity D_5 or D_6 are forward biased. Gate signals of the other two legs are commutating in high-frequency with simultaneous or interleaved command to control half of the sinusoidal input current. A parcel of the converter equivalent inductance is split in the two high-frequency half-bridge legs as they operate in parallel. Input current flows in phase A and only conduction losses exist in D_5 and D_6 because of the low-frequency operation.

Currents in the motor windings are sinusoidal where the input current flows into one phase and goes out by the other two. As the motor is designed to handle higher currents than expected in the charging mode, low conduction losses exist in those windings. Furthermore, as half of the input current is present in two of the three phases lower conduction losses exist compared with the IBC operation proposed by [9]. Detailed information about torque and converter equivalent inductance are discussed in Section III. The active VSC legs control the input current to be sinusoidal and in phase with the input voltage in order to provide unit power factor and low harmonic distortion. The operating modes of the converter are described in the following subsections.

Although one of inverter legs has no commutation losses, the other two are submitted to hard-switching losses including reverse recovery current of antiparallel diodes. It is expected that switches with fast recovery speed are used, as in propulsion mode hard-switching losses are also experienced in the VSC and with higher currents as the traction operation demands higher power. The converter operation is focused on charger mode, however, as a bidirectional converter, energy can be provided from battery to grid in a vehicle-to-grid (V2G) mode. Similar converter operation characteristics would be achieved by providing low-frequency gate signals to the motor winding phase disconnected by the relay, and high-frequency commutation to the other two VSC legs.

A. Operating Modes

The rectifier's operating modes are described based whether the input voltage is positive or negative. An alternative rep-

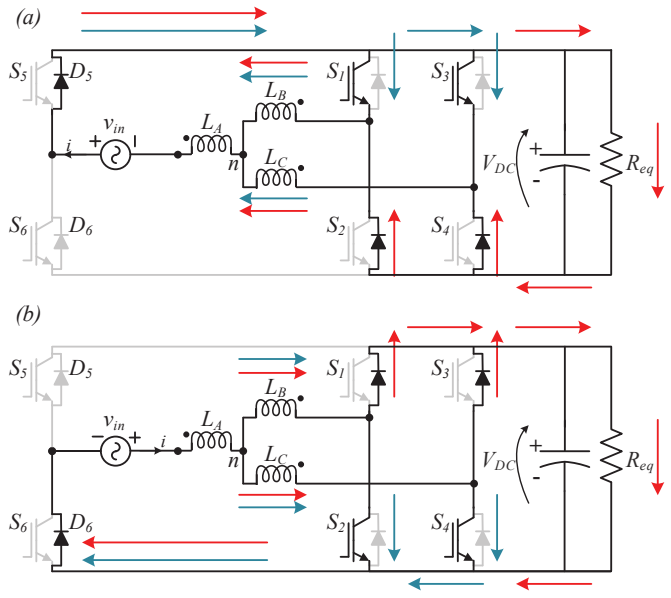

Fig. 2. Stages of operation for the proposed operation mode for the IBC topology. (a) Positive grid voltage. (b) Negative grid voltage.

resentation of the topology is redrawn in Fig. 1b to become clearer the analysis of the proposed IBC operation.

1) Positive Input Voltage: When the input voltage is positive in the adopted reference of Fig. 2a, diode D_5 is forward biased and D_6 is reversed biased. In the figure, blue and red arrows represent first and second stage of operation, respectively. By controlling the switches S_1 and S_3 synchronously, the current i_B and i_C have equal values and the equivalent inductance is accumulating energy. Diode D_6 and antiparallel diodes of S_2 and S_4 withstand the total dc bus voltage. When the gate signal of S_1 and S_3 are commanded to block, the antiparallel diodes of S_2 and S_4 are forward biased and the current through inductors stay in the same direction. Antiparallel diodes of S_1 and S_3 start to block the dc bus voltage. Energy is released from equivalent inductors to dc bus. Diodes D_5 and D_6 do not change their states.

2) Negative Input Voltage: The opposite occurs when the input voltage is negative as the Fig. 2b shows. Diode D_5 is now reversed biased and D_6 is forward biased. Switches S_2 and S_4 are now the active elements and current through inductors is negative. When S_2 and S_4 are commanded to block the antiparallel diodes of S_1 and S_3 are forward biased and the current through inductors stay in the same direction. Antiparallel diodes of S_1 and S_3 are blocking the dc bus voltage in the first stage, and in the second, delivering energy from inductors to dc bus.

B. Static Characteristics

Concerning the rectifier static equations, they can be described as a bridgeless boost converter considering the active switches as an equivalent half-bridge leg with inductance L_B and L_C in parallel. This equivalence holds if the switches of each phase are commutating simultaneously. Considering that

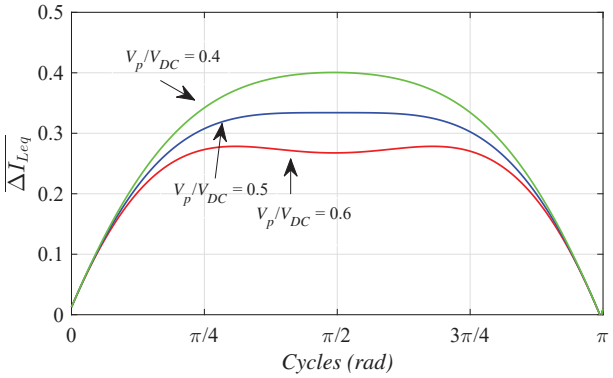

Fig. 3. Parametric current ripple in the equivalent inductance for different values of V_p/V_{DC}.

the equivalent inductance is higher enough to keep the CCM given an input voltage and minimum load condition, the duty cycle is expressed as [13]

$$D(\omega_r t) = \begin{cases} 1 - \dfrac{v_{in}(\omega_r t)}{V_{DC}} & \text{if } v_{in}(\omega_r t) > 0 \\ -\dfrac{v_{in}(\omega_r t)}{V_{DC}} & \text{if } v_{in}(\omega_r t) < 0 \end{cases} \quad (1)$$

where upper case V_{DC} represents output steady state voltage and D is the duty cycle of the equivalent half-bridge leg. Assuming the input voltage has peak value V_p, it is

$$v_{in}(\omega_r t) = V_p \, sin(\omega_r t) \quad (2)$$

Considering the derivative of current in the equivalent inductor in one switching period, the parametric ripple of the input current can be expressed by Eq. 3. As shown by Fig. 3, the point of maximum ripple in one grid period change with the ratio between output and input voltages.

$$\overline{\Delta I_{L_{eq}}} = \frac{L_{eq}\Delta i_{L_{eq}} f_s}{V_p} = sin(\omega_r t) - \frac{V_p}{V_{DC}} sin^2(\omega_r t) \quad (3)$$

Low ripple current is preferable as it reduces the conduction losses and the flux ripple in the machine, thereby implying in reduced iron losses. In the next section the equivalent inductance seen by the rectifier is calculated based on the machine equations.

The winding inductances values are not chosen freely because they depend on the type and construction of machine, so, is necessary to find the minimum acceptable value of equivalent inductance to maintain the converter in CCM during the charging mode in order to decide whether an extra inductance should be added or not. The input current equation can be expressed in terms of the ripple current equation as

$$I_{in} = I_{L,min} + \frac{\Delta i_L}{2} = \frac{P_o \sqrt{2}}{\eta V_{in}} sin(\omega_r t) \quad (4)$$

where P_o represents the output power and η the expected converter efficiency. In the critical conduction mode $I_{L,min}$ is zero, so, the equivalent inductance to guarantee the CCM is determined replacing Eq. 4 and Eq. 3 in Eq. 5.

$$L_{eq} > \frac{\eta V_{in}^2}{2\, P_o\, f_s} \left(1 - \frac{V_p}{V_{DC}} sin(\omega_r t)\right) \quad (5)$$

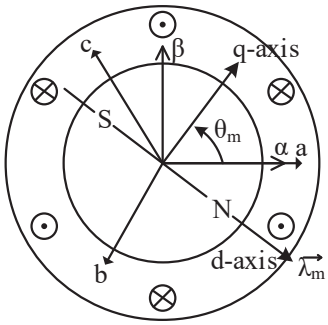

Fig. 4. Adopted reference frame relating abc, $\alpha\beta$ and rotor (dq) axis.

III. Machine Analysis

Electrical motors applied for EV propulsion are often induction or PMSM types. The IMs are robust and cheaper, in contrast, PM motors have higher efficiency and torque density [14]. Both surface-mounted (SPMSM) and interior (IPMSM) PM motors are adopted for traction application.

Based on the motor type and the current applied a three-phase motor can develop torque even in a single-phase charger. In an IBC application, if the motor torque has an average value of zero, not necessarily its instantaneous value will also be zero. Acoustic noise, vibration and lifetime reduction of the mechanical parts could occur in the vehicle caused by the oscillating torque at grid frequency. Lai et al. [15] described the instantaneously developed torque in an SPMSM depending on rotor position for different arrangements of motor windings connection. Here, produced torque for the studied IBC mode of operation is investigated for all three main types of propulsion motors. The equivalent inductance is also calculated from machine equations.

Considering symmetric operation, currents through the windings during charging are described as

$$\begin{aligned} i_A &= I_p\, sin(\omega_r t) \\ i_B &= I_p/2\ sin(\omega_r t + \pi) \\ i_C &= I_p/2\ sin(\omega_r t + \pi) \end{aligned} \tag{6}$$

Changing the reference frame in the machine analysis helps to decouple the rotor position in an induction motor and also decreases the number of equations. Using Clarke's transformation to represent a three-phase reference frame (abc frame) in a two-phase stationary reference frame ($\alpha\beta$ frame), as Eq. 7 shows, gives only an α component of current. The adopted reference frame in a PM motor is illustrated in Fig. 4. Replacing the south and north poles with the rotor windings (or cage) the same representation of axis are valid for the induction machine.

$$\begin{aligned} i_{\alpha,s} &= I_p\, sin(\omega_r t) \\ i_{\beta,s} &= 0 \end{aligned} \tag{7}$$

A. Induction Motor Torque

Stator and rotor equations for a symmetric induction machine in $\alpha\beta$ frame [16] are given by

$$v_{\alpha,s} = r_s i_{\alpha,s} + \frac{d}{dt}\lambda_{\alpha,s} \tag{8}$$

$$v_{\beta,s} = r_s i_{\beta,s} + \frac{d}{dt}\lambda_{\beta,s} \tag{9}$$

$$0 = r_r i_{\alpha,r} - \omega_m \lambda_{\beta,r} + \frac{d}{dt}\lambda_{\alpha,r} \tag{10}$$

$$0 = r_r i_{\beta,r} + \omega_m \lambda_{\alpha,r} + \frac{d}{dt}\lambda_{\beta,r} \tag{11}$$

$$\lambda_{\alpha,s} = (L_{ls} + L_M) i_{\alpha,s} + L_M i_{\beta,r} \tag{12}$$

$$\lambda_{\beta,s} = (L_{ls} + L_M) i_{\beta,s} + L_M i_{\beta,r} \tag{13}$$

$$\lambda_{\alpha,r} = (L_{lr} + L_M) i_{\alpha,r} + L_M i_{\alpha,s} \tag{14}$$

$$\lambda_{\beta,r} = (L_{lr} + L_M) i_{\beta,r} + L_M i_{\beta,s} \tag{15}$$

All variables are referred to the stator side. Subscripts s and r denote respectively a stator and a rotor variable. Winding resistance is r, flux linkage is λ and the angular speed of the rotor is ω_m. The voltages are represented by Eq. 8-11 and the rotor voltages are zero considering a motor with short-circuited rotor windings. Leakage inductances are represented by L_l and the mutual inductance component is related with

$$L_M = 3/2\, L_m \tag{16}$$

where, L_m is the mutual inductance. Being P the number of poles, electromagnetic torque is given by

$$T_e = \frac{3}{2}\frac{P}{2}(\lambda_{\alpha,s}\, i_{\beta,s} - \lambda_{\beta,s}\, i_{\alpha,s}) \tag{17}$$

The zero-torque is achieved if $\lambda_{\beta,s}$ is equal to zero. Replacing Eq. 14 in Eq. 11 gives

$$\frac{d}{dt}\lambda_{\beta,r} + \frac{r_r}{L_M + L_{lr}}\lambda_{\beta,r} = \frac{L_M}{L_M + L_{lr}} i_{\beta,s} - \omega_m \lambda_{\alpha,r} \tag{18}$$

As long as $i_{\beta,s} = 0$ and the rotor is at standstill ($\omega_m = 0$), Eq. 18 can be viewed as a stable first-order differential equation with an equilibrium point of $\lambda_{\beta,r} = 0$, therefore, Eq. 18 proves that $\lambda_{\beta,r}$ will go to and stay at, zero.

Replacing $\lambda_{\beta,r} = 0$ and $i_{\beta,s} = 0$ in Eq. 15 it is obtained that $i_{\beta,r} = 0$. Through Eq. 13 it is shown that $\lambda_{\beta,s}$ is also zero. Finally, by Eq. 17, it is concluded that the electromagnetic torque in an induction machine for the studied IBC is null. This conclusion is independent of the rotor position.

B. PMSM Motor Torque

In a PMSM, voltage equations are equal to Eq. 8 and Eq. 9. However, the rotor flux exists even if there are no stator currents applied. So, with $i_{\beta,s} = 0$, the torque amplitude depends on stator α-axis and rotor flux vector relation.

The stator equations are given by

$$\lambda_{\alpha,s} = L_q i_{\alpha,s} - L_{qd}\, i_{\beta,s} + \lambda_m sin(\theta_m) \tag{19}$$

$$\lambda_{\beta,s} = L_q i_{\beta,s} - L_{qd}\, i_{\alpha,s} + \lambda_m cos(\theta_m) \tag{20}$$

where, θ_m is the electric angular position of the rotor and

$$\begin{aligned} L_q &= L_{ls} + \frac{3}{2}(L_{ms} + L_{mr} cos(2\theta_m)) \\ L_d &= L_{ls} + \frac{3}{2}(L_{ms} - L_{mr} cos(2\theta_m)) \\ L_{qd} &= \frac{3}{2} L_{mr}\, sin(2\theta_m) \end{aligned} \tag{21}$$

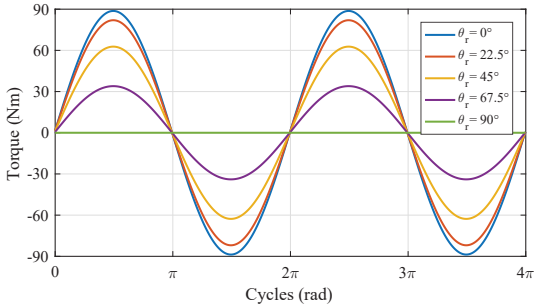

Fig. 5. Developed torque in a SPMSM versus rotor electrical angular position.

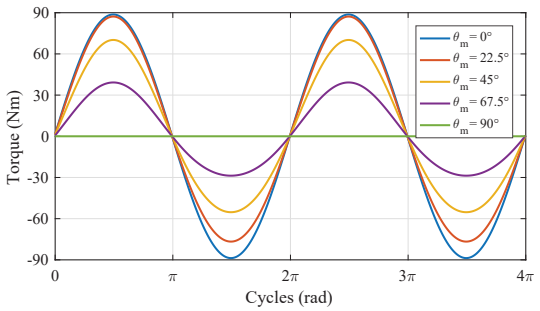

Fig. 6. Developed torque in a IPMSM versus rotor electrical angular position.

Torque equation for a PMSM in the stationary reference frame is equal to Eq. 17. Replacing Eq. 19 and Eq. 20 in Eq. 17 gives

$$T = \left(\frac{P}{2}\right)\left(\frac{3}{2}\right)\left[(L_d - L_q) i_{\alpha,s}\, i_{\beta,s} - L_{qd}(i^2_{\alpha,s} - i^2_{\beta,s}) + \right. \\ \left. + \lambda_m (cos(\theta_m) i_{\alpha,s} - sin(\theta_m) i_{\beta,s})\right] \tag{22}$$

In case of SPMSM application, $L_q = L_d$ and L_{qd} equals to zero. So, the developed torque is equivalent to

$$T = \left(\frac{P}{2}\right)\left(\frac{3}{2}\right) \lambda_m i_{\alpha,s}\, cos(\theta_m) \tag{23}$$

In case of IPMSM, there is an additional component caused by the reluctance. Torque equation is given by

$$T = \left(\frac{P}{2}\right)\left(\frac{3}{2}\right)\left[\lambda_m i_{\alpha,s}\, cos(\theta_m) - 3/2 L_{mr}\, i^2_{\alpha,s}\, sin(2\theta_m)\right] \tag{24}$$

The torque equations as a function of θ_m are illustrated in Fig. 5 and Fig. 6. In both cases, the torque is zero when the rotor flux is aligned with the stator flux, which for the adopted reference occurs when rotor position is 90 degrees.

C. Equivalent Inductance

Although the motor windings can be treated as inductor elements, the proposed configuration does not behave like a conventional converter with separate inductors because they are inversely coupled.

For the IM case, the inductance components that affect the converter equivalent inductance are the leakage inductances of stator and rotor. As a short-circuited transformer, variation of flux in stator leads to current flowing in the rotor. Rotor resistance and leakage inductance are referred to the stator side.

$$L_{eq} = \frac{3}{2}(L_{ls} + L_{lr}) \tag{25}$$

As studied by [15] the equivalent inductance in case of PMSM also depends upon the mutual inductance component and the number of phases in conduction. The voltage equation in phase A is given by

$$v_A = r_r i_A + (L_m + L_{ls})\frac{di_A}{dt} + M_{ab}\frac{di_B}{dt} + M_{ac}\frac{di_C}{dt} \tag{26}$$

As $i_B = i_C = -0.5 i_A$ and because of the three-phase sinusoidally distributed windings the mutual component is represented as $M_{ab} = M_{ac} = -L_m/2$. Thus,

$$v_A = r_r i_A + (\frac{3}{2}L_m + L_{ls})\frac{di_A}{dt} \tag{27}$$

Voltages in phase B and C are the same since they are connected in parallel. Using the same approach, phase B voltage is given by,

$$v_B = r_r i_B + (\frac{3}{2}L_m + L_{ls})\frac{di_B}{dt} \tag{28}$$

As each inductance has value of $3/2L_m + L_{ls}$, the equivalent inductance will be

$$L_{eq} = \frac{9}{4}L_m + \frac{3}{2}L_{ls} \tag{29}$$

This result shows that despite the torque production, compared with solutions based on the Solero configuration [10] which presents equivalent inductance of $L_{ls}/3$, the equivalent inductance of the studied IBC is much higher and can avoid the use of an additional inductance placed between the ac source and the motor. Comparing with operation mode proposed by [9], equivalent inductance is slightly lower as it has value of two times the motor phase inductance. As expressed by Eq. 21 in case of IPMSM the L_m is dependent upon the mechanical rotor position.

IV. Integrated Battery Charger Simulation

Simulation results in MATLAB/Simulink are presented to demonstrate the feasibility of the proposed operation and to verify the developed torque in a motor model with parameters consistent with an EV traction application. A 10-kW charger applied on a 37.3-kW (50 HP) squirrel-cage induction motor with leakage inductance of $L_{ls} = L_{lr} = 867\mu H$ was simulated with variables $i_{L,B}$ and $i_{L,C}$ controlled by two independent PI controllers. Input voltage was 220 V_{rms} and output voltage was set in 400 V. Fig 7 presents all motor winding currents and shows that the instantaneous developed torque for an induction motor is zero, confirming the Section III analysis.

As Fig 8 depicts, the simulation results indicates satisfactory input characteristics as power factor close to unity and current harmonic distortion lower than 5% are obtained. A small current distortion around grid zero-voltage is present. This is typical of bridgeless rectifiers which have the same operation principles of this topology and the response can be improved by non-conventional modulation techniques [13]. A

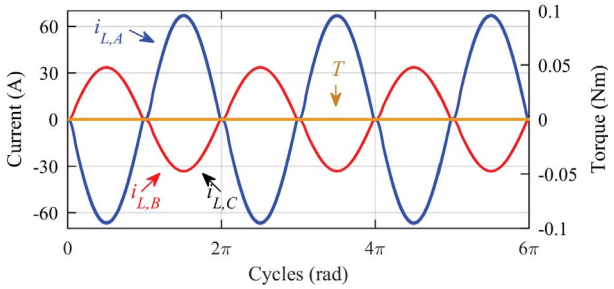

Fig. 7. Simulated waveforms of phase A, phase B and phase C motor winding currents, $i_{L.A}$, $i_{L.B}$, $i_{L.C}$, and torque developed, T, in a induction motor.

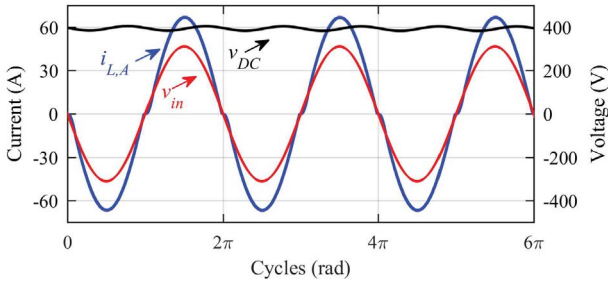

Fig. 8. Simulated waveforms of input voltage v_{in}, phase A motor winding $i_{L,A}$ which is the input current, and output dc bus voltage v_{DC}.

3.3 mF output capacitor was used and a double line frequency component with 5% of voltage ripple is present. With a dc-dc converter as second stage for the battery charger, this voltage ripple can be reduced as well as the dc bus capacitance value and volume.

V. Conclusion

A new operation mode of an integrated onboard inverter/charger for an EV is presented. Comparing with other solutions few additional components are added to the built-in propulsion drivetrain and no special requirements concerning the traction motor are needed. Low-frequency operation of one of the legs allows low commutation losses and full use of the power electronics used in traction. As the input current is shared between two converter legs and motor windings, low conduction losses are also expected.

With the commutation strategy adopted the converter behaves like a bridgeless topology. Detailed analysis are presented regarding the charging operating modes and steady state characteristics including the minimum acceptable inductance value to keep the converter in CCM. As it relies on the motor inductance value, this is not a free parameter to be chosen and the presented equations help to decide whether an additional external inductance is needed or not.

Based on the type of traction machine employed the instantaneously developed torque has different values. Induction motor does not produce torque independently of rotor electric angular position and, due to this, is best suited for the IBC presented. However, in PMSM type, the intantaneous developed zero-torque condition can be achieved if the stator flux is aligned with the magnet rotor flux as demonstrated. Machine equations in $\alpha\beta$ frame are provided to identify the instantaneous torque value with the charger input current characteristic. The equivalent inductance seen by the rectifier converter also changes with the type of motor employed. By using a real model of an induction motor, simulation results prove the feasibility of the proposed charger operation.

Acknowledgment

The authors would like to thank UDESC, FAPESC, CAPES, and FITEJ for the financial support of this work.

References

[1] M. Yilmaz and P. T. Krein, "Review of battery charger topologies, charging power levels, and infrastructure for plug-in electric and hybrid vehicles," *IEEE Transactions on Power Electronics*, vol. 28, no. 5, pp. 2151–2169, May 2013.

[2] W. E. Rippel, "Integrated traction inverter and battery charger apparatus," Apr. 24 1990, US Patent 4,920,475.

[3] M. C. B. P. Rodrigues, I. D. N. Souza, A. A. Ferreira, P. G. Barbosa, and H. A. C. Braga, "Simultaneous active power filter and g2v (or v2g) operation of ev on-board power electronics," in *IECON 2013 - 39th Annual Conference of the IEEE Industrial Electronics Society*, Nov 2013, pp. 4684–4689.

[4] Y. J. Lee, A. Khaligh, and A. Emadi, "Advanced integrated bidirectional ac/dc and dc/dc converter for plug-in hybrid electric vehicles," *IEEE Transactions on Vehicular Technology*, vol. 58, no. 8, pp. 3970–3980, Oct 2009.

[5] S. Kim and F. S. Kang, "Multifunctional onboard battery charger for plug-in electric vehicles," *IEEE Transactions on Industrial Electronics*, vol. 62, no. 6, pp. 3460–3472, June 2015.

[6] S. Haghbin, S. Lundmark, M. Alakula, and O. Carlson, "Grid-connected integrated battery chargers in vehicle applications: Review and new solution," *IEEE Transactions on Industrial Electronics*, vol. 60, no. 2, pp. 459–473, 2013.

[7] D. Thimmesch, "An scr inverter with an integral battery charger for electric vehicles," *IEEE Transactions on Industry Applications*, vol. IA-21, no. 4, pp. 1023–1029, July 1985.

[8] W. E. Rippel and A. G. Cocconi, "Integrated motor drive and recharge system," Mar. 24 1992, uS Patent 5,099,186.

[9] A. Cocconi, "Combined motor drive and battery recharge system," Aug. 23 1994, US Patent 5,341,075.

[10] L. Solero, "Nonconventional on-board charger for electric vehicle propulsion batteries," *IEEE Transactions on Vehicular Technology*, vol. 50, no. 1, pp. 144–149, 2001.

[11] G. Pellegrino, E. Armando, and P. Guglielmi, "An integral battery charger with power factor correction for electric scooter," *IEEE Transactions on Power electronics*, vol. 25, no. 3, pp. 751–759, 2010.

[12] M. Senol and R. W. D. Doncker, "A single-phase, zero-torque, drivetrain integrated on-board charger control method for plug-in hybrid and electric vehicles," in *2015 9th International Conference on Power Electronics and ECCE Asia (ICPE-ECCE Asia)*, June 2015, pp. 863–868.

[13] L. Xue, Z. Shen, D. Boroyevich, and P. Mattavelli, "Gan-based high frequency totem-pole bridgeless pfc design with digital implementation," in *2015 IEEE Applied Power Electronics Conference and Exposition (APEC)*, March 2015, pp. 759–766.

[14] G. Pellegrino, A. Vagati, B. Boazzo, and P. Guglielmi, "Comparison of induction and pm synchronous motor drives for ev application including design examples," *IEEE Transactions on Industry Applications*, vol. 48, no. 6, pp. 2322–2332, Nov 2012.

[15] C. Lai, K. L. V. Iyer, K. Mukherjee, and N. C. Kar, "Analysis of electromagnetic torque and effective winding inductance in a surface-mounted pmsm during integrated battery charging operation," *IEEE Transactions on Magnetics*, vol. 51, no. 11, pp. 1–4, Nov 2015.

[16] P. C. Krause, O. Wasynczuk, S. D. Sudhoff, and S. Pekarek, *Analysis of electric machinery and drive systems*. John Wiley & Sons, 2013, vol. 75.